The non-ribosomal peptide synthetase-independent siderophore (NIS) rhizobactin produced by Caballeronia mineralivorans PML1(12) confers the ability to weather minerals

Cintia Blanco Nouche, Cédric Paris, Tiphaine Dhalleine, Philippe Oger, Marie-Pierre Turpault, Stéphane Uroz

HAL Id: hal-04297012
https://hal.science/hal-04297012

Submitted on 21 Nov 2023

1   **TITLE** : The Non-ribosomal peptide synthetase-Independent Siderophore (NIS) Rhizobactin

2   produced by *Caballeronia mineralivorans* PML1(12) confers the ability to weather minerals

3

4

5

6

7   **AUTHORS :** Cintia Blanco Nouche[1,2], Cédric Paris[3], Tiphaine Dhalleine[1], Philippe Oger[4],

8   Marie-Pierre Turpault[2], Stéphane Uroz[1,2*]

9   [1] Université de Lorraine, INRAE, UMR1136 « Interactions Arbres-Microorganismes », F-

10   54000 Nancy, France

11   [2] INRAE, UR1138 « Biogéochimie des Ecosystèmes Forestiers », F-54280 Champenoux,

12   France

13   [3] Université de Lorraine, EA 4367 « Laboratoire d'Ingénierie des Biomolécules », Ecole

14   Nationale Supérieure d'Agronomie et des Industries Alimentaires (ENSAIA), F-54505

15   Vandœuvre-lès-Nancy, France

16   [4] Université de Lyon, INSA de Lyon, CNRS UMR5240 « Microbiologie, Adaptation et

17   Pathogénie », F-69621, Villeurbanne France

18

19

20

21   **Running title:** Rhizobactin, a new NIS involved in mineral weathering

22

23   *** Corresponding author:** Mailing address: stephane.uroz@inrae.fr

24   Université de Lorraine, INRAE, UMR 1136 "Interactions Arbres Microorganismes", F-54000

25   Nancy, France. Phone: +33 (0)3 83 39 40 81, Fax: +33 (0)3 83 39 40 69.

26

27

SUMMARY

To mobilize nutrients entrapped into minerals and rocks, heterotrophic bacteria living in nutrient-poor environments have developed different mechanisms mainly based on acidolysis and chelation. However, the genetic bases of these mechanisms remain unidentified. To fill this gap, we considered the model strain *Caballeronia mineralivorans* PML1(12) known to be effective at weathering. Based on its transcriptomics and proteomics responses in Fe-depleted conditions we pointed a cluster of genes differentially expressed and putatively involved in the production of siderophores. In this study, we report the characterization of this gene region coding for the production of a Non-ribosomal peptide synthetase (NRPS)-Independent Siderophore (NIS). Targeted mutagenesis associated to functional assays and Liquid Chromatography coupled to High-Resolution tandem Mass Spectrometry (LC-HRMS/MS) demonstrated the production of a single siderophore, identified as rhizobactin. This siderophore represents the first NIS containing malic acid in its structure. The evidence of the implication of the rhizobactin in mineral weathering was demonstrated during a hematite dissolution assay. This study provides the first demonstration of the synthesis of a NIS in the genus *Caballeronia* and its involvement in mineral weathering. Our conclusions reinforce the idea that strain PML1(12) is particularly well adapted to nutrient-poor environments.

45

Keywords: bacteria, mineral weathering, NRPS-independent siderophore, rhizobactin, malic acid

48

49

50   **Importance**

51   This work deciphers the molecular and genetic bases used by the strain PML1(12) of

52   *Caballeronia mineralivorans* to mobilize iron and weather minerals. Through the combination

53   of bioinformatics, chemical and phylogenetic analyses we characterized the siderophore

54   produced by strain PML1(12) and the related genes. This siderophore was identified as

55   rhizobactin and classified as a Non-Ribosomal Peptide Synthetase (NRPS)-Independent

56   Siderophore (NIS). Contrary to the previously identified NIS synthetases that form

57   siderophores containing citric acid, α-ketoglutarate, or succinic acid, our analyses revealed

58   that rhizobactin contains malic acid in its structure, representing therefore the first identified

59   NIS with such acid and probably a new NIS category. Last, this work demonstrates for the

60   first time the effectiveness at weathering minerals of a siderophore of the NIS family. Our

61   findings offer relevant information for different fields of research such as environmental

62   genomics, microbiology and chemistry, as well as soil sciences.

63

INTRODUCTION

Iron represents an essential micronutrient required for living organisms. This element is used as a cofactor by many enzymes and is involved in a wide range of physiological processes such as respiration, DNA synthesis, or photosynthesis [1]. While it is the fourth most abundant element in the Earth crust, it is mainly found under insoluble forms [2,3] in primary (*e.g.,* biotite, granite; Fe^{3+}/Fe^{2+}) and secondary minerals (*e.g.,* hematite, goethite, and magnetite; Fe^{3+}) [4]. In addition, iron is usually poorly bioavailable at neutral to basic pH and under oxygenic conditions. To deal with these limiting conditions and their physiological requirements, bacteria have developed a diversity of mechanisms to mobilize iron and other nutrients poorly available or entrapped into minerals and rocks, a global process termed mineral weathering (MWe).

In heterotrophic bacteria, two main MWe mechanisms have been evidenced: acidolysis and chelation [5]. The first mechanism is related to the action of the by-products of the primary and secondary metabolisms of bacteria. Indeed, by consuming carbon substrates bacteria acidify their local environment due to the production and accumulation of organic acids (*e.g.*, citrate, gluconate) and protons. Such acidification allows the dissolution of the minerals and the release of their nutritive content. The effectiveness of this mechanism is clearly associated to the carbon substrates consumed, with glucose usually giving the stronger acidification [6,7]. The second mechanism is based on the production of chelating compounds such as organic acids (*e.g.,* oxalate) and siderophores. Bacteria can weather minerals using one or both mechanisms (*i.e.*, acidolysis and chelation) depending on the bacterial strain, the nutrient availability, the type of mineral, and the ionic strength of the local environment (*i.e.,* buffering capacity).

Many microorganisms, such as bacteria and fungi, can produce one or more type(s) of siderophore. These particular metabolites are low-molecular weight compounds, characterized

89   by a strong affinity for iron [8], although they can also chelate other divalent and trivalent

90   cations such as Al, Mg or Cr [9,10]. Siderophores are produced when microorganisms

91   experience nutrient limitation and especially iron deficiency [11]. In this sense, concentrations

92   up to 2 and 12 nM of siderophores have been measured in the solution of nutrient-poor soils

93   [12]. To date, two classes of siderophores have been identified: i) the Non-Ribosomal Peptide

94   Synthetase (NRPS) siderophores (*e.g*., pyoverdin), and ii) the NRPS-Independent

95   Siderophores (NIS) (*e.g*., aerobactin) [13]. The contribution of siderophores to MWe has been

96   known for a long time for different types of molecules (*i.e.,* desferrioxamine) in abiotic

97   experiments [14]. However, under such experimental conditions the use of relatively high

98   concentrations of siderophore did not allow to appreciate how microorganisms produced and

99   regulated this production according to their local environment (*i.e*., pH, ionic strength,

100   nutrient availability) [9,15]. Despite a constant increase in the number of new siderophores

101   identified, their role in MWe has rarely been assessed in a cellular context [6,16,17]. Indeed,

102   few studies have considered how the MWe ability of a mutant impaired in siderophore

103   production compares to that of the wild-type strain and how the nutrient limitations impact the

104   action of the siderophore-mediated weathering.

105   In this study we have focused on the model strain PML1(12) from the genus *Caballeronia*

106   *mineralivorans* which has been isolated from a nutrient-poor soil and is known to be effective

107   at MWe and at promoting plant growth [7,18]. However, the molecular basis of its MWe

108   ability is not fully elucidated. The dual transcriptomic and proteomic analyses recently

109   applied on mineral/bacteria interactions highlighted the specific increased expression of a

110   cluster of genes related to iron mobilization and the production of a potential siderophore

111   under Fe depleted conditions [7]. Among these genes the most highly expressed presented

112   high homology with a putative diaminopimelate decarboxylase, cysteine synthase and

113   IucA/IucC synthetase in conditions devoid of iron [7]. In this context, the objectives of this

114   study were to: i) characterize the cluster of genes conferring the ability to mobilize iron of

115   strain PML1(12); ii) purify and characterize the siderophore produced by strain PML1(12);

116   iii) quantify the contribution of siderophore production on mineral weathering; and iv) study

117   the conservation of the genes involved in siderophore production in the *Burkholderia,*

118   *Caballeronia, Paraburkholderia* (BCP) group. To do it, different bioinformatic tools were

119   combined to characterize the cluster of genes related to the production of the NRPS-

120   independent Siderophore (NIS) produced by strain PML1(12) and to determine the relative

121   conservation of this cluster of genes in the genome of different strains from the BCP group.

122   The use of a mutant impaired in its ability to produce the siderophore allowed to determine its

123   role in hematite weathering. Ultra-High Performance Liquid Chromatography coupled with

124   High-Resolution Mass Spectrometry allowed the identification of the chelating molecule.

125

126   **RESULTS**

127   ***A single genomic region is potentially involved in siderophore production***

128   The CAS assay performed on strain PML1(12) demonstrated its ability to mobilize

129   iron as stated by the formation of a yellow halo around the colony, suggesting the production

130   of one or several siderophores. An antiSMASH analysis of the PML1(12) genome identified a

131   single siderophore production locus. This region is characterized by 10 genes, among which a

132   single gene encoding a protein of 635 amino acids, we named RhiE, presenting the

133   characteristic signature of the *iucA/iucC* domain. Such domain is associated to the synthesis

134   of enzymes involved in the production of NRPS-Independent Siderophores (NIS). The other

135   genes present in the region upstream and downstream of the *rhiE* gene could be involved in

136   siderophore production (*rhiBCD*, intermediate production of the siderophore), transport (*rhiA,*

137   TonB transporter; *rhiF*, MFS transporter; *rhiGHI,* ABC systems) and in the regulation of

138   siderophore production (*rhiJ*). The detail of the functions encoded by each gene of the

139   *rhiABCDEFGHIJ* cluster is presented in Table 1.

140

141   ***The rhiABCDEFGHIJ region confers the ability to mobilize iron to strain***

142   ***PML1(12)***

143   To investigate the implication of this region in siderophore biosynthesis, a *rhiE*::Gm

144   knock-out mutant was constructed and tested on solid CAS assay to compare its siderophore

145   production with that of the WT strain (Figure S1). After seven days of incubation, the WT

146   strain presented a yellow halo of *ca.* 1.7 cm, while no halo was visible for the *rhiE*::Gm

147   mutant strain. The lack of production of chelating molecules by the *rhiE*::Gm mutant strain

148   was confirmed with the liquid CAS assay, which showed a very slight $O.D._{655nm}$ decrease

149   from 0.48 ± 0.01 to 0.43 ± 0.01 between the non-inoculated treatment and the *rhiE*::Gm

150   mutant, when the decrease reached a final value of 0.11 ± 0.01 for the WT strain indicative of

151   a trapping of iron from the CAS-Fe(III) complex.

152

153   ***The rhiABCDEFGHIJ cluster permits the growth of strain PML1(12) in iron***

154   ***deficient condition***

155   The growth capabilities of the WT and *rhiE*::Gm strains were measured in a medium

156   devoid of iron (ABm-Fe) amended or not with various concentrations of iron (0, 0.5, 1, 5 and

157   10 $mg.L^{-1}$ of Fe) (Figure 1). In absence of iron, the growth of the WT strain was delayed and

158   reached a maximum $O.D._{595nm}$ value of 0.58 ± 0.01. The growth rate in absence of iron was

159   significantly lower ($P < 0.05$) than that observed in the presence of iron at 5 or 10 $mg.L^{-1}$

160   concentration ($O.D._{595nm} = 0.88 \pm 0.01$). The *rhiE*::Gm mutant strain reached the same

161     $O.D._{595nm}$ as the WT strain when growing at the highest iron concentrations (*i.e.*, 5 and 10

162     $mg.L^{-1}$), but with an important growth delay. The maximal $O.D._{595nm}$ was observed at 50h vs.

163 26h for the *rhiE*::Gm and WT strains, respectively. The largest growth differences (*i.e.*,

164 maximal O.D.$_{595nm}$ and delay) between WT and *rhiE*::Gm strains were observed when iron

165 concentrations were below 1 mg.L^{-1} in the solution.

166

167 ***Inhibition of the siderophore production according to Fe concentration***

168 As the production of chelating molecules is usually dependent on Fe concentration in

169 the medium, we assayed the production of siderophores in a range of concentrations of Fe

170 from 0 to 5 mg.L^{-1}. After a 3-day incubation period in ABm-Fe amended or not with iron (*i.e.,*

171 FeCl$_3$), the analyses done on the culture supernatant revealed the lack of chelating activity in

172 the non-inoculated controls and in the WT cultures in presence of iron concentrations at 0.8

173 mg.L^{-1} (Figure 2), while this activity was detectable at 0.7 mg.L^{-1} and below. Chelating

174 activity reached its maximum in absence of iron in the medium. The same experiment

175 performed with the *rhiE*::Gm mutant did not reveal any chelating activity whatever the iron

176 concentration tested.

177

178 ***Hematite weathering***

179 The ability of the chelating molecule(s) produced by strain PML1(12) to weather

180 minerals was evaluated considering hematite, an iron-rich mineral, as the sole source of iron

181 in our experimental conditions. To limit the impact of acidification on the mineral weathering

182 process, experiments were done in buffered ABm-Fe medium over 7 days of incubation. The

183 pH of the medium was controlled before and after the experiments in presence/absence of

184 bacterial inoculum and hematite and remained stable (pH = 6.1). In absence of hematite, the

185 WT strain grew in the buffered ABm-Fe medium to an O.D.$_{595nm}$ = 0.47 ± 0.01. The presence

186 of hematite in the medium significantly increased growth of the WT strain (O.D.$_{595nm}$ = 0.82 ±

187 0.01), while hematite addition had no impact on growth of the *rhiE*::Gm mutant (O.D.$_{595nm}$ =

188 0.45 ± 0.01 in presence vs. O.D.$_{595nm}$ = 0.44 ± 0.02 in absence of the mineral). The CAS assay

189 confirmed that only the WT strain was presenting an active chelating activity in both

190 conditions (*e.g.*, in the presence or in the absence of hematite). Quantification of the iron

191 released in solution from hematite highlighted significantly higher concentrations of iron for

192 the WT strain ([Fe]= 0.76 ± 0.02 mg.L^{-1}; P<0.05) than for the *rhiE*::Gm mutant (0.04 ± 0.02

193 mg.L^{-1}) and the non-inoculated control (0.06 ± 0.02 mg.L^{-1}) (Figure 3).

194

195 ***Rhizobactin is the siderophore produced by strain PML1(12)***

196 Pre-purified supernatants from 3-day cultures of *rhiE*::Gm mutant and WT strains

197 were analyzed by HPLC after purification. For this experiment, the growth was performed in

198 ABs-Fe with succinate as sole carbon source to limit the production of exopolysaccharides,

199 which are not compatible with the purification steps. The comparison of the HPLC

200 chromatograms from the WT and *rhiE*::Gm strains as well as from the medium alone

201 highlighted one major difference, a peak (peak #1) with a retention time (RT) of 0.84 min in

202 the WT supernatant. This peak was 2.8 and 3.8 times more intense for the WT strain than for

203 the *rhiE*::Gm mutant strain and the non-inoculated medium, respectively (Figure 4A). To

204 correlate the HPLC chromatograms with the presence of chelating activities, the HPLC

205 fractions were collected and assayed using the CAS assay. The CAS assay was positive for

206 two fractions for the WT samples. The first positive fraction with the CAS assay (O.D.$_{655nm}$ =

207 0.06) was collected between 0.77 and 0.97 min corresponding to peak #1 region. The second

208 positive fraction (O.D.$_{655nm}$ = 0.14) was identified between 3.74 and 3.95 min. Detailed

209 analysis of the HPLC profiles within this retention time highlighted the presence of a small

210 peak (peak #2), only for WT strain (Figure 4B).

211 To identify the siderophore produced by strain PML1(12), we performed a HPLC-

212 PDA-HRMS/MS analysis of the two fractions mentioned above. High resolution MS analysis

213 revealed the presence of a single molecule with the same exact mass of 377.1868 Da

214 (monoprotonated ion seen at m/z = 378.1868) in both active fractions and with the theoretical

215 formula $C_{15}H_{25}O_8N_3$ (Figure 5A). Such compound was found only in the WT fractions (and

216 not in the *rhiE*::Gm strain, nor in the negative control). An additional MS signal with m/z =

217 431.0982 was also specifically observed in the two active WT fractions and was

218 unambiguously attributed to the ferric complex $[(C_{15}H_{25}O_8N_3\text{-}2H) + {}^{56}Fe(III)] + (m/z_{theo} =$

219 377.1788-2 × 1.008 + 55.935 = 431.0978, with ${}^{56}Fe = 55.935$ u and ${}^1H = 1.008$ u). Indeed, the

220 experimental isotopic pattern was in perfect agreement with the simulated one (Figure 6),

221 thanks to the clear observation of the contribution of ${}^{54}Fe$ isotope at m/z = 429.1029

222 $([(C_{15}H_{25}O_8N_3\text{-}2H) + {}^{54}Fe(III)]^+)$. The previous mass spectrometric observations allow to

223 conclude with certainty that compound of exact mass M = 377.1788 Da can bind iron (III)

224 efficiently and corresponds to the siderophore produced by strain PML1(12).

225 Such exact mass of 377.1868 Da has been previously associated to the siderophore

226 rhizobactin by Smith *et al.* [19] in a strain of *Ensifer meliloti* and Kügler *et al.* [20] in the

227 strain *Pseudomonas* sp. FEN. In order to elucidate the siderophore highlighted in PML1(12),

228 a tandem mass spectrometry experiment (MS/MS) was performed (Figure 5B). Noticeably,

229 our analyses identified the same four major product ions characterizing the rhizobactin

230 described by Kügler *et al.* [20] (Figure 5C) as : i) m/z = 289.1351 (formed as a result of loss

231 of alanine), ii) m/z = 200.0882 (formed as a result of loss of ethylenediamine and alanine and

232 an additional carboxylic group), iii) m/z = 116.0681 (identified as malic acid ion) and iv) m/z

233 = 84.0790 (identified as decarboxylated lysine ion). Overall, these analyses demonstrate that

234 PML1(12) produces rhizobactin, a siderophore composed of a lysine, an alanine, an

235 ethylenediamine group and malic acid. This work represents the first demonstration that

236 rhizobactin is a NRPS-independent siderophore. Furthermore, it confirms that rhizobactin is

237 based on malic acid and not on other known NIS substrates (citric acid, α-ketoglutarate, or

238 succinic acid).

239

240   *Comparative genomics of rhizobactin synthesis*

241   A BlastP search of the nr database using the RhiE protein as template allowed the

242 identification of several homologous proteins presenting a percentage of identity ranging from

243 64% to 85% and good sequence coverage (95 to 100%). The best hits appeared assigned to

244 the genera *Paraburkholderia, Trinickia, Vogesella, Polaromonas* or *Pseudomonas*.

245 Noticeably, a homologue was found in strain FEN of *Pseudomonas sp.* (63.5% homologue to

246 RhiE; NCBI accession number WP_191487624.1), a strain described previously for its ability

247 to produce rhizobactin, but in which the synthesis genes had not been identified. Focusing on

248 the *Burkholderiaceae*, we identified 38 proteins presenting a percentage of identity ranging

249 from 34% to 85% and belonging to the genus *Paraburkholderia*, *Trinickia*, *Cupriavidus* and

250 *Ralstonia.* Considering the BCP group, besides the homologues in *Caballeronia*, we found

251 RhiE homologues only in 5 strains assigned to *Paraburkholderia (sp.* BL23I1N*, P.*

252 *haematera, P. sp.* T12-10*, P. sp.* NMBU_R16 and P. *sp*. Ac-20340), organized almost

253 identically as in PML1(12) (*i.e.,* cluster *rhiABCDEFJ*) (Figure 7), but with a variable number

254 of genes. Noticeably, the ABC transport systems were not always present.

255   The phylogenetic analysis of NIS synthetases usually clusters them according to their

256 substrate specificity [13]. To position the RhiE synthetase of strain PML1(12) in the NIS

257 classification and to determine its relatedness to the known NIS synthetases, we constructed a

258 N-J phylogenetic tree of a representative set of known NIS synthetases (Figure 8). A total of

259 24 protein sequences of NIS synthetases which function, and substrate, are known were

260 considered, as well as RhiE protein sequence of PML1(12) and the two homologous RhiE

261 protein sequences identified in *Pseudomonas* FEN and *Ensifer (Sinorhizobium) meliloti* AK83

262 which are also potentially involved in rhizobactin production. Overall, our results confirm that

263 NIS synthetases are distributed according to their substrate specificity [13,21-23]. The newly

264 characterized RhiE NIS synthetase of strain PML1(12), as well as the two homologues from

265 *Pseudomonas* and *Ensifer*, cluster in group A', forming a well-supported sub-branch within

266 this group. Cluster A' is the only in the phylogeny which does not seem to follow substrate

267 specificity. Indeed, as demonstrated in the current work, RhiE and homologues synthesize

268 rhizobactin, which is based on the use of malic acid as substrate (see above), while others NIS

269 from this cluster use citric acid to synthesize siderophores such as rhizoferrin. The low

270 support of the tree at the base of this cluster (bootstrap values of 37 and 42) may indicate a

271 problem of phylogenetic resolution using the current set of data.

272 The comparison of the complete genomic region of the cluster of genes involved in

273 rhizobactin transport and production (*rhiABCDEFGHIJ*) (Table 1) found in strain PML1(12)

274 with the genomes of the strains already known to produce rhizobactin (*Ensifer meliloti* and

275 *Pseudomonas* sp. FEN) highlighted a partial conservation of this cluster (*i.e., rhiBCDEF*).

276 The clusters differed however in several instances: i) the presence of a TonB system in the

277 upstream region in strain PML1(12) and at the downstream end in strain AK83

278 (AEG58212.1) and ii) the absence of two ABC-transport systems (*rhiHI*) and the

279 transcriptional regulator (*rhiJ*) in strains AK83 and FEN (Figure 7).

280

281 **DISCUSSION**

282 **Rhizobactin identification**

283 Rhizobactin was first described in the plant-associated bacterial strain *Ensifer meliloti*

284 DM4 (former *Sinorhizobium meliloti*) [19]. This first study provided a detailed chemical

285 composition based on mass spectrometry and NMR analyses, revealing that this carboxylate

286 siderophore was formed by an ethylenediamine group coupled with alanine, lysine, and malic

287 acid. The same siderophore was reported more recently for a bacterial strain isolated from a

288 nutrient-poor environment, the strain *Pseudomonas sp.* FEN [20]. Both studies provided the

289 chemical characterization of this molecule, but neither the genetic characterization nor the

290 classification of rhizobactin. Interestingly, *Pseudomonas sp.* FEN can produce rhizobactin and

291 rhizobactin B, rhizobactin B being the main siderophore produced. Structurally, these two

292 siderophores differ only by the presence of a methyl group at the C2 position of malic acid,

293 giving a citramalic acid in rhizobactin B instead of a malic acid in rhizobactin. A third

294 rhizobactin type was identified in strain 1021 of *Ensifer meliloti* (*i.e.,* rhizobactin 1021), but

295 completely different in terms of chemical structure from the one described above. This

296 hydroxamate siderophore of 530 Da is based on a citrate derivative with the carboxyl groups

297 linked to two different side chains [23]. In our study, we identified the siderophore produced

298 by strain PML1(12) using a combination of CAS assay, HPLC purification and MS/MS

299 analyses. This molecule not only binds the different iron isotopes but also presented an exact

300 mass (377.1868 Da) and a fragmentation pattern like that of the rhizobactin identified in

301 *Ensifer meliloti* strain DM4 and *Pseudomonas sp.* strain FEN [19,20]. Our *rhiE*::Gm mutant

302 of strain PML1(12), which is unable to chelate iron, proves the involvement of the *rhiE* gene

303 cluster in the production of the unique siderophore molecule produced by strain PML1(12).

304 Noticeably, the rhizobactin gene cluster appeared relatively conserved in the two strains

305 already described for the production of rhizobactin, though the strain *Pseudomonas sp.* FEN

306 presented an additional gene identified as a citrate lyase (WP_191487621.1), which is the first

307 gene of the cluster in this strain, upstream of the *rhiE* homologue. Citrate lyase, may be

308 involved in the process of transformation of malic acid into citramalic acid, explaining why

309 rhizobactin B is the main siderophore produced by strain *Pseudomonas sp.* FEN, while

310 rhizobactin is produced by *Ensifer meliloti* AK83 and strain PML1(12).

311

Rhizobactin as NRPS-Independent Siderophore

Two groups of bacterial siderophores are currently described according to their biosynthetic pathway. The first pathway uses complex, modular, multidomain enzymes known as NRPS [6,13,24]. The second relies on NRPS-independent synthetases [13,25]. In comparison to the wealth of information available on the genetics and chemistry of the NRPS siderophores, NIS and their related biosynthetic pathways are still poorly documented [25]. This is an important point because siderophores cannot be categorized as NIS or NRPS without a proper genetic characterization. In this sense, rhizobactin was discovered and chemically characterized by Smith *et al*. [19], as early as 1984, in strain *Ensifer meliloti* DM4, but could only be classified as a NIS thanks to the current study and its homology at chemical ($C_{15}H_{25}O_8N_3$) and genomic level (gene cluster) to that of strain PML1(12). The strain PML1(12) presents a gene cluster of 10 genes (Figure 7) with the characteristic signature of the NIS synthesis pathway as identified for the first described NIS (*i.e*., aerobactin) [26, 27]. The aerobactin-synthetases, *iucA* and *iucC* became since that, the hallmarks of the presence of NIS in genomes [22], either in a single copy such as for the synthesis of rhizoferrin (*e.g.,* FslA) in *Francisella tularensis* [28] or rhizobactin in strain PML1(12) (*e.g*., RhiE, this study) or either in several copies such as for the synthesis of aerobactin (*e.g.,* IucA and IucC) [27]. Our findings will enrich the NIS database and improve the siderophore determination using AntiSMASH.

Rhizobactin a new class of NIS?

NIS synthetases traditionally separate in five phylogenetic groups (A, A', B, C and C'). This classification which was obtained on experimentally demonstrated NIS synthetases is congruent with their substrate specificity with: i) type A and A' specific for citric acid; ii) type B for α-ketoglutarate intermediates; and iii) type C and C' specific for citryl or succinyl-

337 based intermediates [13]. The number of experimentally demonstrated NIS synthetases is

338 limited and consequently their position in phylogenetic trees may change with the evolution

339 of NIS studies. As an example, the SfaB and SfaD enzymes responsible for the synthesis of

340 Staphyloferrin A which presents a citric acid in its structure [29] were initially included in

341 group B, a group of NIS synthetases specific for α-ketoglutarate. With the discovery of other

342 novel citric acid-based and chiral siderophores (*e.g.*, rhizoferrin, legiobactin) SfaB and SfaD

343 now cluster within a new group, named A'. Our phylogenetic tree agrees with those

344 previously published [13,21,22], confirming that the NIS synthetases mostly cluster according

345 to their substrate specificity. In this respect, the rhizobactin synthetase clusters with group A',

346 which corresponds to citrate-based and chiral siderophores. However, rhizobactin and

347 rhizobactin B synthetases form a well-supported branch within group A'. Malic acid

348 (rhizobactin) and citramalic acid (rhizobactin B) have never been described previously as

349 possible substrates for NIS synthetases. Therefore, the difference of substrate specificity

350 between rhizobactin synthetases (malic for rhizobactin and citramalic acid for rhizobactin B)

351 and synthetases from group A' (citric acid), and the absence of other already characterized

352 synthetases with malic acid as substrate, allow us to propose a new group of NIS called D.

353 The future characterization of new NIS synthetases that use malic/citramalic acid as substrate

354 should make more robust the separation from A' group, as it happened previously for groups

355 B and A' [29].

356

357 **Role of rhizobactin in mineral weathering**

358 Iron is considered as an essential element and its deficiency alters the growth of

359 bacteria [6,30,31]. Strain PML1(12) follows this rule, with a strong delay and decrease in

360 growth in iron deprived conditions compared to non-limiting conditions. To adapt to low-iron

361 conditions, bacteria can produce siderophores, whose production is regulated by the quantity

362   of iron available and stopped at a maximum of 5 mg.L^{-1} of Fe [32]. Here, we showed that the

363   production of rhizobactin by strain PML1(12) was detectable until an iron concentration of

364   0.7 mg.L^{-1}. Such iron regulation fits with the observations done by the dual transcriptomic and

365   proteomic analyses on strain PML1(12) in the presence/absence of a mineral carrying iron

366   (*i.e.,* biotite), which evidenced that the genes involved in siderophore production were only

367   up-regulated in Fe-depleted conditions and in the absence of mineral [7]. Although minerals

368   represent an important source of iron, the production of siderophores remains strongly

369   determined by the iron bioavailability and the local conditions (pH, ionic strength). Several

370   studies have demonstrated that in oligotrophic conditions minerals may be seen as a source of

371   iron if siderophore-producing bacteria are present in the environment [33]. The effectiveness

372   of siderophores at solubilizing iron from different minerals is known and demonstrated for a

373   long time in abiotic conditions. As an example, desferrioxamine B was proved to weather Fe

374   from several iron oxides [15]. Even more, rhizoferrin and desferrioxamine A and B are not

375   only effective at mobilizing Fe from hydroxide minerals, but also other metals such as

376   chromium [34,35]. However, such abiotic experiments were usually based on high

377   concentrations of siderophores and did not permit to consider all the regulation occurring in

378   bacteria according to nutrient availability, ionic strength of the medium and mineral type. In

379   contrast, few studies investigated the ability of siderophore-producing bacteria to liberate

380   nutrients trapped in minerals in a cellular context, considering mutants impaired in their

381   ability to produce siderophores. Our study represents the first demonstration of the role of a

382   NIS (*i.e.*, rhizobactin) produced in biotic conditions in the weathering of hematite. Such

383   demonstration completes the list of siderophores already characterized for their role in

384   mineral weathering [6,16,17,33].

385

386   **Occurrence of the Rhizobactin siderophore in the BCP group**

387   Among members of the same genus or species, the type of siderophore produced can

388   strongly differ (*i.e.*, rhizoferrin biosynthesis) [36,37] or on the contrary be very conserved

389   (*i.e.,* pyoverdine biosynthesis)[38]. Members of the *Burkholderia sensu lato* are well known

390   for the different strategies they use to mobilize iron based on siderophore-independent (Ftr)

391   [39] and siderophore-dependent (*e.g.,* ornibactin) [40,41] systems, but not yet based on a NIS.

392   Our study represents the first evidence of the production of rhizobactin in this group. Based

393   on this evidence, we evaluated the distribution of a homologue of the *Caballeronia*

394   *mineralivorans* strain PML1(12) RhiE NIS synthetase and the conservation of the *rhi* cluster

395   of genes. Our analysis revealed that homologues of RhiE can be found in many genera among

396   Beta-proteobacteria, but the most represented remains the *Pseudomonas* genus. In this

397   context, *Pseudomonas sp.* FEN is the only strain characterized for its ability to produce

398   rhizobactin, while many *Pseudomonas* strains have been described for their ability to produce

399   NRPS siderophores (*e.g.,* pyoverdin) [38]. Focusing on the BCP group (including

400   *Burkholderia, Paraburkholderia* and *Caballeronia*), only five *Paraburkholderia* strains (*P.*

401   sp. BL23I1N*, P. haematera,* sp. T12-10*, P.* sp. NMBU_R16 and *P.* sp. Ac-20340) presented

402   the rhizobactin cluster, questioning its origin. In terms of ecology, many of the strains we

403   identified to possess a rhizobactin synthesis locus homologue originate from the rhizosphere

404   (*e.g., Paraburkholderia sp.* T12-10, R16 and Ac-20340 and most of the members of *Trinickia,*

405   *Vogesella, Polaromonas* or *Pseudomonas*) and nutrient-poor ecosystems suggesting a role in

406   plant nutrition and adaptation to nutrient-poor conditions. The role of siderophore-producing

407   bacteria in plant nutrition and growth promotion has already been demonstrated as in the case

408   of the strains *Burkholderia pyrrocinia* JK-SH007 [40] or *Caballeronia mineralivorans*

409   PML1(12) [42,43].

410

411   **Conclusion**

412   It is clearer and clearer that the ability of bacteria to weather minerals is finely

413   regulated by local conditions and physiological processes. Nutrient availability, ionic strength

414   of the medium and the type of mineral and of the carbon substrate metabolized, strongly

415   determine the mechanism used by bacteria and the effectiveness at weathering. While the

416   global mechanisms are identified (*i.e.*, acidification, chelation, oxido-reduction), the genetic

417   and geochemical bases remain poorly documented. Demonstrations in a cellular context (*i.e.*,

418   effect of a gene mutation) are essential to cover without *a priori* the diversity of mechanisms

419   used by phylogenetically different bacteria and to decipher the regulations of these

420   mechanisms occurring according to the mineral type and the local conditions. The

421   combination of molecular and (geo-)chemical techniques used here not only allowed the

422   identification of the siderophore produced by strain *Caballeronia mineralivorans* PML1(12)

423   as rhizobactin, but also its classification as an NRPS-independent siderophore (NIS) and its

424   contribution to mineral weathering. Our study provides new information regarding the

425   complexity of mechanisms used by this model strain according to the local conditions and its

426   metabolism. Our results highlight that siderophores play an essential role in mineral

427   weathering under buffered and non-acidifying conditions, while organic acid and proton-

428   based mechanisms represent the main mineral weathering mechanism used by this strain

429   under non-buffered and acidifying conditions. The ability of rhizobactin to weather more

430   complex and less weatherable minerals, with a lower iron content (*e.g.,* biotite) remains to be

431   determined. Together, our results clearly highlight how the strain PML1(12) is well adapted

432   to live in nutrient-poor environments and to develop complex and finely regulated

433   mechanisms to mobilize nutrients from minerals.

434

435   **MATERIALS AND METHODS**

436   **Bacterial strains and growth media**

437   Bacterial strains and plasmid are listed in Table 2. The model *Caballeronia*

438 *mineralivorans* strain PML1(12) was isolated from the ectomycorrhizosphere of *Scleroderma*

439 *citrinum* associated with oak (for sampling details see Calvaruso *et al*. [44])

440   Strains, with the exception of *Escherichia coli*, were grown in AB medium [45]

441 supplemented with mannitol (ABm) or succinic acid (ABs) (2 g.L^{-1} final concentration) at 25

442 °C. A version of the AB medium devoid of iron was also used (AB-Fe). *E. coli* strains were

443 grown in Luria-Bertani (LB) at 37 °C. When required, gentamycin, kanamycin and ampicillin

444 were added to the media at a final concentration of 20, 50 and 100 μg.mL^{-1}, respectively.

445

446   *Preparation of bacterial inoculum of Caballeronia mineralivorans* strain PML1(12)

447 and its mutant

448   For each of the assays presented in this work, the wild-type (WT) strain and the

449 *rhiE*::Gm mutant strain were recovered from glycerol stock (-80 °C) and grown on solid ABm

450 medium (25 °C) for 2 days. One isolated colony of each strain was inoculated in 10 mL of

451 liquid ABm medium and incubated 3 days at 25 °C under 150 rpm agitation. Liquid cultures

452 were centrifugated at 9000 g for 15 min at 4 °C and the pellet was washed three times with

453 sterile MilliQ water. The pellet was resuspended in sterile MilliQ water, and the optical

454 density was adjusted to O.D.$_{595nm}$= 0.9 ± 0.03 (corresponding to 2.10^9 cell/mL).

455

456   **rhiE::Gm mutant construction**

457   Total DNA was extracted from the WT strain PML1(12) using the protocol of

458 Pospiech and Neumann [46]. To construct a targeted mutant of the gene homologous to

459 *iucA/iucC* (*rhiE*), the total gene was amplified using a combination of primers including For-

460 *rhiE* and Rev-*rhiE* for a complete amplification and Rev-*rhiE_Sma*I and For-*rhiE_Sma*I to

461 insert a *Sma*I site (Table 2; Figure S2 for details). The insertion of a *Sma*I site in the middle of

462   the *rhiE* gene was done following 3 PCR rounds: i) For-*rhiE* with Rev-*rhiE_Sma*I (967 bp),

463   ii) For-*rhiE_Sma*I with Rev-*rhiE* (966 bp) and iii) For-*rhiE* and Rev-*rhiE* (1908 bp). The PCR

464   products of PCR1 and 2 were purified and used as matrix for PCR 3. After amplification and

465   purification, PCR3 product was ligated into the pGEM-T Easy plasmid (Promega) resulting in

466   the plasmid pGEM-*rhiE_Sma*I (Table 2). The plasmid pGEM-*rhiE_Sma*I was then digested

467   with *Sma*I to introduce the *Sma*I-digested gentamycin (Gm) resistance cassette from plasmid

468   pUC1318, resulting in the plasmid pGEM-*rhiE*::Gm. A fragment containing the *rhiE*::Gm

469   cassette was then obtained by *Eco*RI restriction and cloned in the plasmid pK19mob, resulting

470   in the pK19mob-*rhiE*::Gm plasmid. This construction was transferred to *E. coli* S17.1λpir and

471   then to strain PML1(12) by bi-parental conjugation. Δ*rhiE* mutants were recovered after 5

472   days of incubation at 25 °C on gentamycin-containing ABm plates. The transconjugants

473   obtained were verified by PCR with For-*rhiE* and Rev-*rhiE* primers, to differentiate the single

474   and double cross-over events. Several single and double-cross-over mutants were obtained

475   and conserved. The experiments described in our study were done using a double cross-over

476   mutant named *rhiE*::Gm.

477

478   **Siderophore activity**

479   Siderophore activity was detected using the liquid and solid versions of the Chrome

480   Azurol S (CAS) assay according to Schwyn and Neilands [47]. For both assays, the color

481   change, sign of the chelating activity of the siderophore for the iron (III) of the CAS-Fe

482   complex can be quantified by the presence of a halo on the solid CAS assay or through the

483   measurement of the optical density (O.D.) at 655 nm for the liquid assay.

484   For the solid CAS assay, 5 µL of the bacterial inoculum (both WT and mutant strains;

485   corresponding to 5.10^6 colonies forming unit (CFU)) were inoculated in triplicate in agar

486 plates and incubated three days at 25 °C. The diameter of colony and the halo surrounding it

487 were measured to determine growth and siderophore(s) production, respectively.

488 For the liquid CAS assay, 0.5 mL of the bacterial inoculum (both WT and mutant

489 strains; corresponding to 5.10^8 CFU) were inoculated in triplicate in 4.5 mL ABm-Fe. After 3-

490 days incubation at 25 °C under agitation (150 rpm), the cultures were centrifuged at 9000 g

491 during 15 min at 4 °C to recover culture supernatants. A volume of 100 µL of these

492 supernatants were mixed with 100 µL of CAS-Fe(III) and incubated during 1h at room

493 temperature in the dark. Then, the O.D. was measured at 655 nm using a microplate reader

494 (Bio-Rad, model iMark). Decrease of absorbance at this specific wavelength is synonym of

495 siderophore presence (change of media coloration from blue to yellow [6, 47]). Non-

496 inoculated medium was used as negative control for the liquid assay.

497

498 **Impact of iron concentration on the growth the WT and *rhiE*::Gm strains**

499 To determine if the concentration of iron and the mutation of the *rhiE* gene (*rhiE*::Gm

500 mutant) affected the growth of strain PML1(12), growth was determined at different iron

501 concentrations (*i.e.,* 0, 0.5, 1, 5, 10 mg.L^{-1} of Fe). A bacterial inoculum of 10 µL

502 (corresponding to 6.10^6 CFU) was added to 190 µL of ABm-Fe and incubated in 96-well

503 microplates for 5 days. This experience was performed in triplicate and conducted at 25 °C on

504 orbital shaking in a microplate reader (Tecan infinite M200 pro). The absorbance was

505 measured at 595 nm every 3 hours. To evaluate the growth of the strains, the slope of the

506 exponential phase (*i.e.*, growth rate) was calculated for each condition and replicate.

507

508 **Siderophore production inhibition**

509 Siderophore production is known to be regulated by the availability of nutritive

510 elements in the culture medium, especially iron. To evaluate the concentration of Fe necessary

511   to inhibit the siderophore production, the WT and mutant strains were incubated at different

512   iron concentrations. Non-inoculated conditions were used as negative controls for each

513   concentration. A volume of 10 µL of inoculum was added to 180 µL of ABm-Fe

514   supplemented with 10 µL of different $FeCl_3$ stock solutions ranging from 0 to 5 mg.L^{-1} of Fe

515   to obtain the following final concentrations in the medium: 0, 0.1, 0.2, 0.3, 0.4, 0.5, 0.6, 0.7,

516   0.8, 0.9, 1, 1.5, 2, 2.5, 5 mg.L^{-1}. The 96-well microplates were incubated 3 days at 25 °C.

517   Then, microplates were centrifugated at 3000 g during 15 minutes at 4 °C and 100 µL of

518   supernatant were mixed with 100 µL of CAS-Fe(III). After 1 h incubation in the dark the

519   plates were read at 655 nm using a microplate reader (Bio-Rad, model iMark) as described

520   above.

521

522   **Hematite weathering assay**

523   *Hematite characteristics*

524   Hematite (Fe_2O_3) is an iron-oxide mineral widely distributed in all soils [48] and

525   characterized by a high iron content. The hematite used in this study comes from a batch

526   extracted in Brazil. The chemical composition was determined on crushed powder by

527   inductively coupled plasma-atomic emission spectrometry (700 Series ICP-AES, Agilent

528   Technologies) as described in Picard *et al.* [49]. This analysis revealed that the hematite used

529   is mainly composed of Fe_2O_3 (99.3%) and also contains in small amounts: 0.40% TiO_2, 0.18%

530   SiO_2, 0.16% Al_2O_3, 0.10% MgO, 0.037% MnO.

531

532   *Mineral weathering assay*

533   To avoid contamination by residues associated with glass tubes, all glassware was

534   rinsed once with 3.6% HCl and then three times with MilliQ water. The tubes were filled with

535   200 mg of hematite and 9 mL of ABm-Fe medium and autoclaved at 121 °C. To evaluate the

536   differences in the weathering ability of the *rhiE*::Gm mutant and the WT strains, 1 mL of each

537   inoculum was added to the tubes (procedure performed in triplicate). Non-inoculated media

538   with and without hematite were used as abiotic and sterility controls for weathering. Samples

539   were incubated for 7 days under agitation at 150 rpm and 25 °C.

540   The cultures were used to determine: i) bacterial growth, ii) solution pH, iii)

541   siderophore production and iv) iron concentrations. Bacterial growth was estimated directly

542   on the liquid culture by measuring the O.D.$_{595nm}$ on 200 µL. The other measurements were

543   done after centrifugation at 14000 g for 15 min to remove bacterial cells and hematite

544   particles. A volume of 100 µL of supernatant was used to evaluate the level of siderophore(s)

545   production using the liquid CAS assay according to the protocol described above. A volume

546   of 180 µL of supernatant was used to measure the pH by mixing with 20 µL of bromocresol

547   green (1 g.L^{-1}) according to [18]. For the measure of the iron concentration, the supernatant

548   was filtered at 0.22 µm (GHP Acrodisc 25 mm syringe filter; PALL) before mixing 180 µL of

549   supernatant with 20 µL of ferrospectral. Both pH and iron determinations are based on optical

550   density measurements at 595 nm using a microplate reader (Bio-Rad, model iMark) and after

551   conversion with the calibration curves done on the bromocresol green and ferrospectral dyes,

552   according to [18].

553

554   **Chemical characterization of the siderophore**

555   *Siderophore production and purification*

556   Volumes of 50 mL of ABs-Fe were inoculated with each strain (WT and *rhiE*::Gm)

557   and incubated at 25 °C under 150 rpm shaking for three days. Succinic acid was used here as

558   sole carbon source to limit the production of exopolysaccharides. A non-inoculated condition

559   was also included as negative control. After the incubation time, cultures were centrifugated

560   at 9000 g, during 15 min at 4 °C. The supernatant was filtered using 0.45 µm filters

561 (Millipore) and treated with a Sep pack Vac 6cc tC18 Cartridge (Waters) to pre-purify and

562 concentrate the siderophore(s). The columns were first washed with 10 mL of 100% ethanol

563 and then equilibrated with 10 mL of 0.01% trifluoroacetic acid (TFA). After this equilibration

564 step, a volume of 25 mL of supernatant was added progressively to the column and finally the

565 different fractions of the supernatant were eluted by the addition of 5 mL of 10% and then

566 20% methanol in water. At each step the eluted volume (*ca.* 5 mL) was recovered and

567 concentrated in the SpeedVac system. The dried samples were resuspended in 100 µL of

568 MilliQ water. These pre-purified fractions were used for further characterization using the

569 liquid CAS assay to verify the presence of siderophore.

570

571 *High Performance Liquid Chromatography (HPLC) analyses and fractionation*

572 The different pre-purified fractions recovered above (from WT, mutant and negative

573 control samples) were analyzed by HPLC. A volume of 50 µL of each extract was injected in

574 a Gemini C18 column (150 x 3.0 mm, 5 µm particle size, Phenomenex). Solvent A consisted

575 of MilliQ water and solvent B consisted of acetonitrile plus 0.2% of TFA. A linear gradient

576 elution from 2% to 40% of solvent B over 25 min at a flow rate of 1 mL.min^{-1} was used to

577 separate compounds. Absorbance was monitored at 210 nm.

578 Peaks of potential interest were identified by comparing the chromatogram of the WT

579 sample with that of the *rhiE*::Gm mutant sample and the negative control. To determine the

580 presence of the siderophore(s) activity, a fraction collection was performed in 96-wells

581 microplates using a fraction collector system (FRC-10A fraction collector system, Shimadzu).

582 Fractions of 200 µL were recovered each 0.2 s using the same HPLC conditions as described

583 before. Fraction collection was performed three times independently, and fractions with the

584 same retention times were pooled. The fractions collected were then concentrated using the

585 SpeedVac and resuspended in 100 µL of MilliQ water. To determine the presence of

586   siderophore(s) activity, a volume of 25 µL of the collected fractions was mixed with 25 µL of

587   liquid CAS and the absorbance at 655 nm was measured after overnight incubation.

588

589   *Qualitative HPLC-DAD-MS-MS/MS analysis of siderophores and ferrosiderophores*

590   A Thermo Scientific UHPLC-HRMS/MS system composed of a Vanquish™ liquid

591   chromatography unit coupled to a photodiode array detector (PDA) and an Orbitrap ID-X™

592   Tribrid™ high-resolution mass spectrometer operating in electrospray ionisation mode (ESI)

593   was used to detect and identify the putative siderophores. Ten microliters of each bacterial

594   extract were injected onto a Hichrom Alltima C18 column (150×2.1 mm - 5 µm) maintained

595   at 25 °C. The flow rate was set at 0.2 mL.min^{-1} and mobile phases consisted in water modified

596   with formic acid (0.1%) for A and acetonitrile modified with formic acid (0.1%) for B.

597   Compounds of interest were eluted using a linear gradient from 5% to 20% of B for 10 min,

598   then a 5 min isocratic step was applied at 98% of B to wash the column, before returning to

599   the initial composition of 5% B for 6 min to reach the equilibrium. Mass analysis was carried

600   out in ESI positive ion mode (ESI^{+}) and mass spectrometry conditions were as follows: spray

601   voltage was set at 3.5 kV; source gases were set (in arbitrary units.min^{-1}) for sheath gas,

602   auxiliary gas and sweep gas at 35, 7 and 10, respectively; vaporizer and ion transfer tube

603   temperatures were both set at 300 °C. Survey scans of precursors were performed from 150 to

604   2000 m/z at 60 K resolution (FWHM at 200 m/z) with MS parameters as follows: RF-lens,

605   35%; maximum injection time, 50 ms; data type, profile; internal mass calibration EASY-IC

606   TM activated; normalized AGC target: 25%. A top speed data dependent MS^2 (0.6 sec for the

607   whole cycle time) was carried out using a wide quadrupole isolation (1.5 Th), a HCD

608   fragmentation with a stepped collision energy (20, 35 and 50%) and an Orbitrap measure at

609   15 K resolution (high-resolution MS/MS analysis). Precursors with an intensity upper than

610   2.10^4 were automatically sampled for MS^2. Dynamic exclusion was used, and the time of

611 exclusion was set at 2.5 s, with a 10 ppm tolerance around the selected precursor (isotopes

612 excluded). Other MS^2 parameters were as follows: data type, profile; normalized AGC target:

613 20%; AGC target, 10000.

614   Mass spectrometer calibration was performed by using the Thermo Scientific Pierce

615 TM FlexMix TM calibration solution. MS data acquisition was carried out by using the

616 Xcalibur v. 3.0 software (Thermo Scientific).

617

618   **Bioinformatic analyses**

619   *Genome analysis*

620   Genome analysis was performed using MicroScope MaGe (Magnifying Genomes)

621 [50] and NCBI. The presence of *iucA/iucC* gene homologue was identified by antiSMASH

622 [51] and confirmed by BLASTP analyses based on sequence homology [52].

623

624   *Phylogenetic analyses*

625   A total of 27 protein sequences (Table S1) homologous to IucA/IucC, including the

626 homologue of PML1(12) (RhiE), were recovered from NCBI to build a phylogenetic

627 Neighbor-Joining (N-J) tree using the Seaview platform (version 5.0.4)[53]. For this analysis,

628 the protein sequences considered were: i) sequences which role in siderophore biosynthesis

629 were experimentally demonstrated; ii) sequences based on their homology with the RhiE

630 protein identified in strain PML1(12). Protein sequences were aligned using MUSCLE

631 algorithm and then a N-J tree with 100.000 iterations was constructed.

632

633   **Statistical analyses.**

634   Statistical analyses were performed in R software (Tidyverse packages)[54]. Triplicate

635   samples were used in all experiments. Differences between samples means (pH, growth, CAS

636   assay and released iron) or growth slopes were analyzed by ANOVA and TukeyHSD tests.

637

647

648   **References**

649   1. Andrews SC, Robinson AK, Rodríguez-Quiñones F. 2003. Bacterial iron

650   homeostasis. *FEMS Microbiol Ecol* 27: 215-237.

651   2. Desai A, Archana G. 2011. Role of Siderophores in Crop Improvement. *Bacteria*

652   *in Agrobiology: Plant Nutrient Management* 109–139.

653   3. Radzki W, Gutierrez Mañero FJ, Algar E, Lucas García JA, García-Villaraco A,

654   Ramos Solano B. 2013. Bacterial siderophores efficiently provide iron to iron-

655   starved tomato plants in hydroponics culture. *ALJMAO* 104: 321–330.

656   4. Colombo C, Palumbo G, He JZ, Pinton R, Cesco S. 2014. Review on iron

657   availability in soil: interaction of Fe minerals, plants, and microbes. *J Soils*

658   *Sediments* 14: 538–548.

659 5. Uroz S, Picard P, Turpault MP. 2022. Recent progress in understanding the
660   ecology and molecular genetics of soil mineral weathering bacteria, *Trends*
661   *Microbiol* 30: 882-897.

662 6. Picard L, Paris C, Dhalleine T, Morin E, Oger P, Turpault MP, Uroz S. 2022. The
663   mineral weathering ability of *Collimonas pratensis* PMB3(1) involves a
664   Malleobactin-mediated iron acquisition system. *Environ Microbiol* 24: 784-802.

665 7. Uroz S, Picard L, Turpault MP, Auer L, Armengaud J, Oger P. 2020. Dual
666   transcriptomics and proteomics analyses of the early stage of interaction between
667   *Caballeronia mineralivorans* PML1(12) and mineral. *Environ Microbiol* 22: 3838-
668   3862.

669 8. Neilands JB. 1995. Siderophores: structure and function of microbial iron transport
670   compounds. *J Biol Chem* 270: 26723-26726.

671 9. Kraemer SM, Duckworth OW, Harrington JM, Schenkeveld WDC. 2015.
672   Metallophores and Trace Metal Biogeochemistry. *Aquat Geochem* 21:159–195

673 10. Shiny Matilda C, Mannully ST, Rao VP, Shanti C. 2021. Chromium binding
674   *Bacillus cereus* VITSH1 - a promising candidate for heavy metal clean up. *Lett*
675   *Appl Microbiol* 72: 517-525.

676 11. Kramer J, Özkaya Ö, Kümmerli R. 2020. Bacterial siderophores in community and
677   host interactions. *Nat Rev Microbio* 18: 152-163.

678 12. Essén SA, Bylund D, Holmström SJ, Moberg M, Lundström US. 2006.
679   Quantification of hydroxamate siderophores in soil solutions of podzolic soil
680   profiles in Sweden. *Biometals* 19: 269-282.

681 13. Carroll, C.S. and Moore, M.M. (2018). Ironing out siderophore biosynthesis: a
682   review of non-ribosomal peptide synthetase (NRPS)-independent siderophore
683   synthetases. *Crit Rev Biochem Mol Biol* 53: 4, 356-381

684   14. Torres MA, Dong S, Nealson KH, West AJ 2019. The kinetics of siderophore-
685   mediated olivine dissolution. *Geobiol* 17: 401-416.

686   15. Cheah SF, Kraemer SM, Cervini-Silva J, Sposito G. 2003. Steady-state dissolution
687   kinetics of goethite in the presence of desferrioxamine B and oxalate ligands:
688   Implications for the microbial acquisition of iron. *Chem Geol* 198: 63–75.

689   16. Dehner CA, Awaya JD, Maurice PA, DuBois JL. 2010. Roles of siderophores,
690   oxalate, and ascorbate in mobilization of iron from hematite by the aerobic
691   bacterium *Pseudomonas mendocina*. *Appl Environ Microbiol* 76: 2041–2048.

692   17. Parrello D, Zegeye A, Mustin C, Billard P. 2016. Siderophore-Mediated Iron
693   Dissolution from Nontronites Is Controlled by Mineral Cristallochemistry. *Front*
694   *Microbiol* 7: 423.

695   18. Uroz S, Calvaruso C, Turpault MP, Pierrat JC, Mustin C, Frey-Klett P.
696   2007. Effect of the Mycorrhizosphere on the Genotypic and Metabolic Diversity of
697   the Bacterial Communities Involved in Mineral Weathering in a Forest Soil. *Appl*
698   *Environ Microbiol* 73: 3019–3027.

699   19. Smith MJ, Shoolery JN, Schwyn B, Holden I, Neilands JB. 1985. Rhizobactin, a
700   structurally novel siderophore from Rhizobium meliloti. *J Am Chem Soc* 107:
701   1739–1743.

702   20. Kügler S, Cooper RE, Boessneck J, Küsel K, Wichard T. 2020. Rhizobactin B is
703   the preferred siderophore by a novel *Pseudomonas* isolate to obtain iron from
704   dissolved organic matter in peatlands. *Biometals* 33: 415–433.

705   21. Challis GL. 2005. A widely distributed bacterial pathway for siderophore
706   biosynthesis independent of nonribosomal peptide synthetases. *Chem biochem* 6:
707   601-611.

708   22. Oves-Costales D, Kadia N, Challis GL. 2009. The long-overlooked enzymology
709   of a nonribosomal peptide synthetase-independent pathway for virulence-
710   conferring siderophore biosynthesis. *Chem Commun* 43: 6530-6541.

711   23. Persmark M, Pittman P, Buyer JS, Schwyn B, Gill Jr PR, Neilands JB. 1993.
712   Isolation and structure of rhizobactin 1021, a siderophore from the alfalfa
713   symbiont *Rhizobium meliloti* 1021. *J Am Chem Soc* 115: 3950–3956.

714   24. Budzikiewicz H. 1997. Siderophores of fluorescent pseudomonads. *Z Naturforsch*
715   *C J Biosci* 52: 713–720.

716   25. Barry SM, Challis GL. 2009. Recent advances in siderophore biosynthesis. *Curr*
717   *Opin Chem Biol* 13: 205-215.

718   26. Bindereif A, Neilands JB. 1983. Cloning of the aerobactin mediated iron
719   assimilation system of plasmid ColV. *J Bacteriol* 153: 1111–1113.

720   27. De Lorenzo V, Bindereif A, Paw BH, Neilands JB. 1986. Aerobactin biosynthesis
721   and transport genes of plasmid colV-K30 in *Escherichia coli* K-12. *J Bacteriol*
722   165: 570–578.

723   28. Ramakrishnan G, Pérez NM, Carroll C, Moore MM, Nakamoto RK, Fox TE.
724   2019. Citryl Ornithine Is an Intermediate in a Three-Step Biosynthetic Pathway for
725   Rhizoferrin in *Francisella*. *ACS Chem Biol* 14: 1760-1766.

726   29. Cotton JL, Tao J, Balibar CJ. 2009. Identification and characterization of the
727   *Staphylococcus aureus* gene cluster coding for staphyloferrin A. *Biochemistry* 48:
728   1025-1035.

729   30. Dehner CA, Barton L, Maurice PA, DuBois JL. 2011. Size-dependent
730   bioavailability of hematite (α-Fe2O3) nanoparticles to a common aerobic
731   bacterium. *Environ Sci Technol* 45 : 977-983.

732 31. Mridha S, Kümmerli R. 2022. Coordination of siderophore gene expression among

733   clonal cells of the bacterium *Pseudomonas aeruginosa*. *Commun Biol* 5: 545.

734 32. Dave BP, Dubc HC. 2000. Regulation of siderophore production by iron Fe(III) in

735   certain fungi and fluorescent pseudomonads. *Indian J Exp Biol* 38: 297–299.

736 33. Van Den Berghe M, Merino N, Nealson KH, West AJ. 2021. Silicate minerals as a

737   direct source of limiting nutrients: Siderophore synthesis and uptake promote ferric

738   iron bioavailability from olivine and microbial growth. *Geobiolog* 19: 618-630.

739 34. Akafia MM, Harrington JM, Bargar JR, and Duckworth OW. (2014). Metal

740   oxyhydroxide dissolution as promoted by structurally diverse siderophores and

741   oxalate. *Geochim Cosmochim Acta* 141: 258–269.

742 35. Duckworth OW, Akafia MM, Andrews MY, Bargar JR. 2014. Siderophore-

743   promoted dissolution of chromium from hydroxide minerals. *Environ Sci Process*

744   *Impacts* 16: 1348-1359.

745 36. Carroll CS, Grieve CL, Murugathasan I, Bennet AJ, Czekster CM, Liu H,

746   Naismith J, Moore MM. 2017. The rhizoferrin biosynthetic gene in the fungal

747   pathogen *Rhizopus delemar* is a novel member of the NIS gene family. *Int J*

748   *Biochem Cell Biol* 89: 136-146.

749 37. Sullivan JT, Jeffery EF, Shannon JD, Ramakrishnan G. 2006. Characterization of

750   the siderophore of *Francisella tularensis* and role of *fslA* in siderophore

751   production. *J Bacteriol* 780: 3785-3795.

752 38. Schalk IJ, Rigouin C, Godet J. 2020. An overview of siderophore biosynthesis

753   among fluorescent Pseudomonads and new insights into their complex cellular

754   organization. *Environ microbiol* 22: 1447-1466.

755 39. Mathew A, Eberl L, Carlier AL. 2014. A novel siderophore-independent strategy

756   of iron uptake in the genus *Burkholderia*. *Mol microbiol* 91: 805-820.

757 40. Min L, Guo L, Ye J. 2019. Mechanism of *Burkholderia pyrrocinia* JK-SH007

758   growth-promoting to plant via siderophore-mediation. *Journ Nanjing Forest Univ*

759   *Nat Sci Ed* 43: 165-172.

760 41. Alice AF, Lopez CS, Lowe CA, Ledesma MA, Crosa JH. 2006. Genetic and

761   transcriptional analysis of the siderophore malleobactin biosynthesis and transport

762   genes in the human pathogen *Burkholderia pseudomallei* K96243. *J Bacteriol* 188:

763   1551–1566.

764 42. Calvaruso C, Turpault MP, Frey-Klett P. 2006. Root-associated bacteria contribute

765   to mineral weathering and to mineral nutrition in trees: a budgeting analysis. *Appl*

766   *Environ Microbiol* 72: 1258-1266.

767 43. Koele N, Turpault MP, Hildebrand EE, Uroz S, Frey-Klett P. 2009. Interactions

768   between mycorrhizal fungi and mycorrhizosphere bacteria during mineral

769   weathering: budget analysis and bacterial quantification. *Soil Biol and Biochem*

770   41: 1935-1942.

771 44. Calvaruso C, Turpault MP, Leclerc E, Frey-Klett P. 2007. Impact of

772   ectomycorrhizosphere on the functional diversity of soil bacterial and fungal

773   communities from a forest stand in relation to nutrient mobilization processes.

774   *Microb Ecol* 54: 567–577.

775 45. Chilton MD, Currier TC, Farrand SK, Bendich AJ, Gordon MP, Nester EW. 1974.

776   *Agrobacterium tumefaciens* DNA and PS8 bacteriophage DNA not detected in

777   crown gall tumors. *Proc Natl Acad Sci* 71: 3672–3676.

778 46. Pospiech A, Neumann B. 1995. A versatile quick-prep of genomic DNA from

779   gram-positive bacteria. *Trends in genetics: TIG*, 11 : 217-218.

780 47. Schwyn B, Neilands JB. 1987. Universal chemical assay for the detection and

781   determination of siderophores. *Anal Biochem* 160: 47–56.

782   48. Dixon JB, Weed SB, Dinauer RC. (eds) 1989. Minerals in soil environments, 2nd
783   ed. Madison, WI, USA: Soil Science Society of America.

784   49. Picard L, Turpault MP, Oger P, Uroz S. 2021. Identification of a novel type of
785   glucose dehydrogenase involved in the mineral weathering ability of *Collimonas*
786   *pratensis* strain PMB3(1). *FEMS Microbiol Ecol* 97: fiaa232.

787   50. Vallenet D, Calteau A, Dubois M, Amours P, Bazin A, *et al*. 2019. MicroScope:
788   an integrated platform for the annotation and exploration of microbial gene
789   functions through genomic, pangenomic and metabolic comparative analysis.
790   *Nucleic Acids Res* 4: D579–D589.

791   51. Blin K, Shaw S, Kloosterman AM, Charlop-Powers Z, van Weezel GP, Medema
792   MH, Weber T. 2021. antiSMASH 6.0: improving cluster detection and comparison
793   capabilities. *Nucleic Acids Res* 2: 29-35.

794   52. Altschul SF, Gish W, Miller W, Myers EW, Lipman DJ. 1990. Basic local
795   alignment search tool. *J Mol Biol* 215: 403-410.

796   53. Gouy M, Guindon S, Gascuel O. 2010. SeaView version 4: a multiplatform
797   graphical user interface for sequence alignment and phylogenetic tree building.
798   *Mol Biol Evol* 27: 221-224.

799   54. R Core Team (2021). R: A language and environment for statistical computing. R
800   Foundation for Statistical Computing, Vienna, Austria. URL

801

802

803 **Figure Legends.**

804

805 **Figure 1. Growth assay.** The growth of the WT strain (**A**) and *rhiE*::Gm mutant (**B**) was

806 monitored in presence of different iron concentrations (*i.e.,* 0, 0.5, 1, 5, 10 mg.L^{-1} of Fe) in AB

807 medium depleted of iron. The growth was studied under orbital shaking at 25 ºC for 90 h. The

808 absorbance was measured at 600 nm every 3 hours. Each dot is the mean of independent

809 triplicates.

810

811 **Figure 2. Impact of increasing concentrations of iron on the chelating activity of the WT**

812 **and mutant (*rhiE*::Gm) strains.** To determine the concentration of iron inhibiting

813 siderophore production, liquid cultures of WT (red) and *rhiE*::Gm (blue) strains were

814 performed with different concentrations of iron (*i.e.,* 0, 0.1, 0.2, 0.3, 0.4, 0.5, 0.6, 0.7, 0.8, 0.9,

815 1, 1.5, 2, 2.5, 5 mg.L^{-1}). Pure water (grey) was used as a negative control. After 3 days, the

816 absorbance at 655 nm was measured. The decrease of the measured absorbance means the

817 presence of chelating molecules since the media coloration changes from blue to yellow and

818 the absorbance measured at 655 nm measures blue color intensity.

819

820 **Figure 3. Hematite weathering potential of strain PML1(12) and its *rhiE*::Gm mutant.**

821 The weathering ability was evaluated by the measure of iron released from hematite in ABm

822 medium devoid of iron, after 7 days of incubation at 25 °C under agitation (200 rpm). (**A**)

823 **Concentration of iron released in solution**. The iron released from hematite was measured

824 by ferrospectral determination (optical density measured at 595_{nm}). Abbreviations were used

825 as follows: WT + H, wild type strain plus hematite; WT, wild type strain; *rhiE*::Gm + H,

826 mutant strain plus hematite; *rhiE*::Gm, mutant strain; abiotic + h, non-inoculated condition

827 plus hematite; abiotic, non-inoculated condition. Non-inoculated conditions (abiotic control

34

828   with and without hematite) were used as controls. Samples with the same letter indicate no

829   significant difference (P<0.05). **(B) Siderophore activity**. The siderophore activity of the

830   different samples was determined using the CAS method. The yellow color indicates

831   siderophore activity. For each measure, the results are the mean of independent triplicates.

832

833   **Figure 4**. **HPLC analysis and UV detection.** The pre-purified supernatant of the WT strain

834   (red), *rhiE*::Gm mutant (blue) and non-inoculated medium (grey) were monitored at 210 nm

835   after HPLC separation using a Milli-Q water / acetonitrile + 0.2% TFA gradient for 25 min at

836   1 mL.min^{-1}. To determine the presence of siderophore activity, fractions were collected during

837   the HPLC run and tested using the liquid CAS assay. Positive fractions for siderophore

838   presence are highlighted with black arrows. **(A)** A major peak (peak 1) at retention time of

839   0.84 min was identified. **(B)** A second peak (peak 2) of lower intensity, with a retention time

840   of 3.88 min , was identified after CAS test.

841

842   **Figure 5. Identification, fragmentation profile and chemical structure of rhizobactin. (A)**

843   Mass spectrum of HPLC positive fractions showing the parent ion of the putative chelating

844   molecule at m/z=378.1868 (raw formula: $C_{15}H_{25}O_8N_3$). **(B)** Fragmentation pattern of the

845   chelating molecule seen at m/z=378.1868, revealing a perfect agreement with previous

846   experimental MS^2 results done on the rhizobactin identified in *Sinorhizobium meliloti* DM4

847   by Smith *et al.* (1985) and in *Pseudomonas sp*. FEN by Kügler *et al.* (2020). The major

848   product ions are: 289.1351 (in blue, consecutive to alanine loss), 200.0882 (in yellow, formed

849   as a result of loss of ethylenediamine and alanine and an additional carboxylic group),

850   116.0681 (in red, corresponding to malic acid ion - H_2O) and 84.0790 (in green,

851   corresponding to decarboxylated lysine ion) **(C)** Chemical structure (according to Smith *et al.,*

852   1985) and fragmentation pattern of the rhizobactin. Same colors as in panel A are used to

853   highlight the correspondence of the chemical moieties of rhizobactin and product ions. Dotted

854   boxes are used to highlight lost ions while undotted boxes mark the remaining structure of the
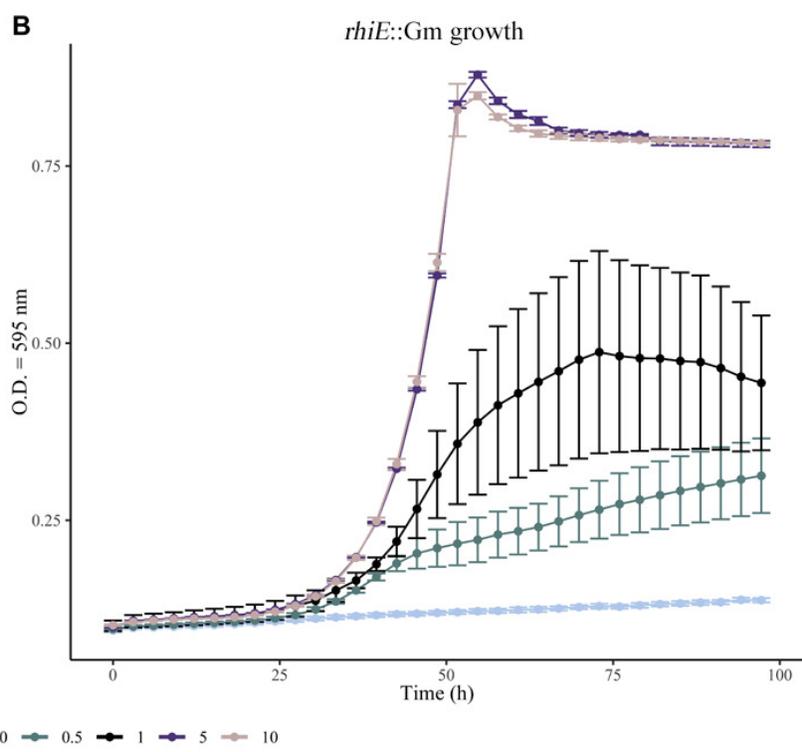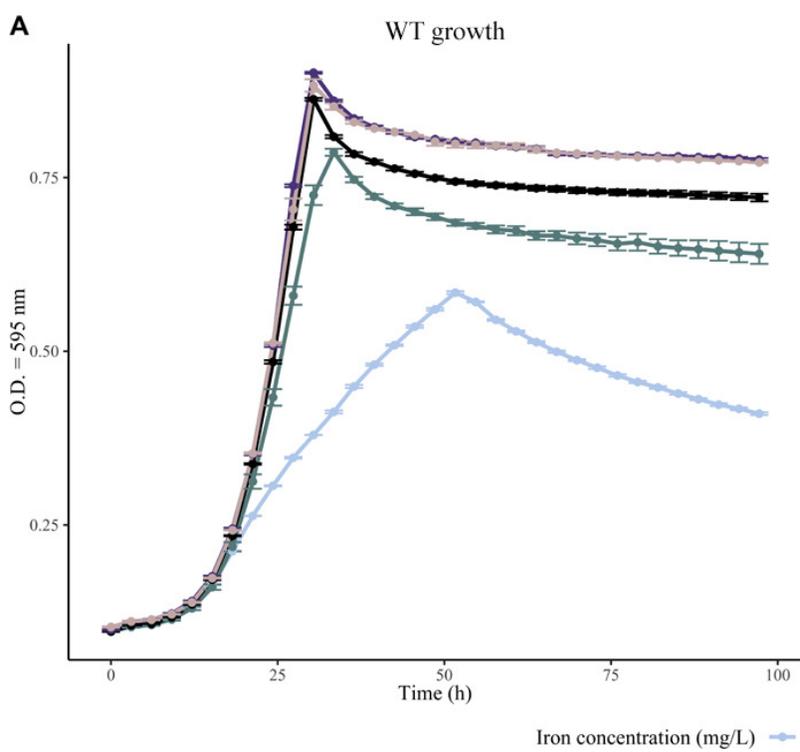
855   molecule.

856

857

858   **Figure 6. Isotopic pattern of iron complexes**. Comparison between **(A)** the experimentally

859   observed isotopic pattern of the putative iron(III) siderophore complex ion (m/z=431.0963),

860   and **(B)** the theoretical isotopic profile of the complex $[(C_{15}H_{25}O_8N_3\text{-}2H)+Fe^{III}]^+$, $C_{15}H_{25}O_8N_3$

861   being the raw formula associated with the putative siderophore of m/z=378.1868.

862

863   **Figure 7. Organization of the cluster of genes involved in rhizobactin biosynthesis in**

864   **different strains**. Each arrow represents one gene, and its size was scaled according to gene

865   length. Gene annotation is shown in the right and the complete description is provided in

866   Table 1. Light grey, dark grey and green genes are involved in siderophore transport. In blue,

867   red, and yellow, genes are involved in siderophore biosynthesis. In black, genes involved with

868   siderophore production regulation. In bold, strains for which rhizobactin synthesis was
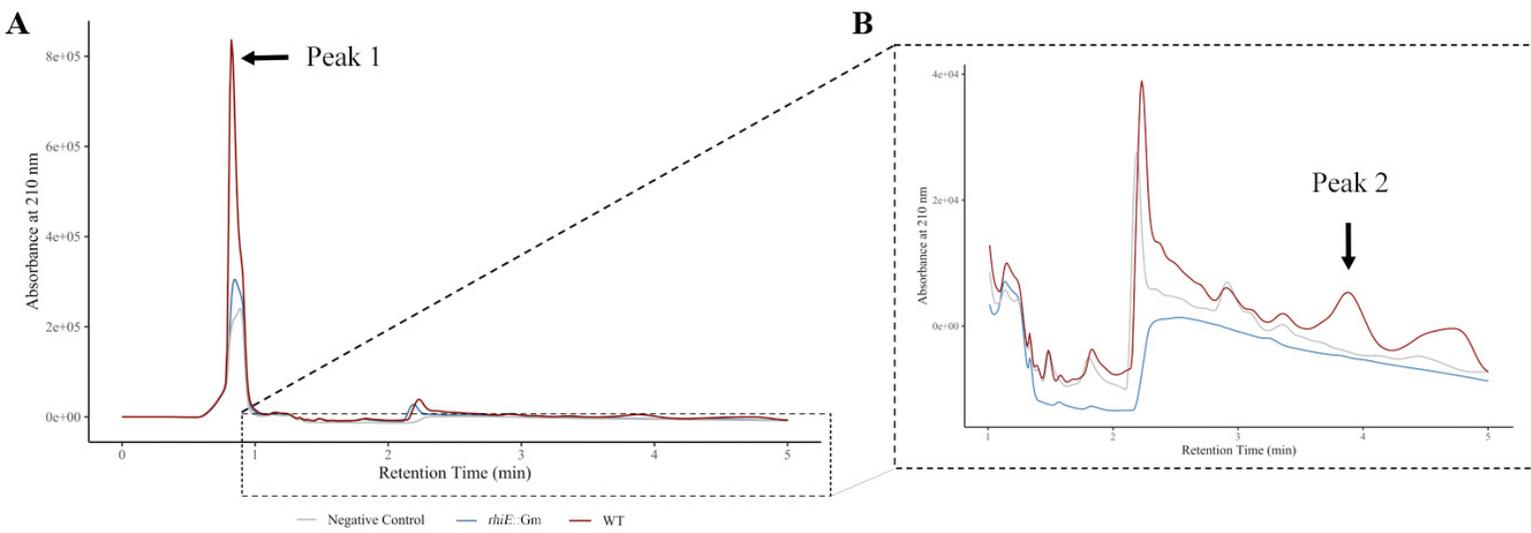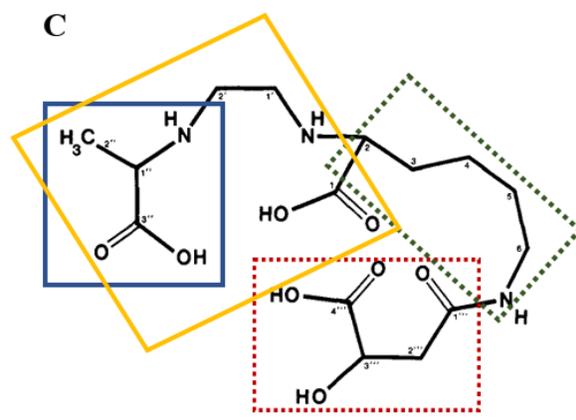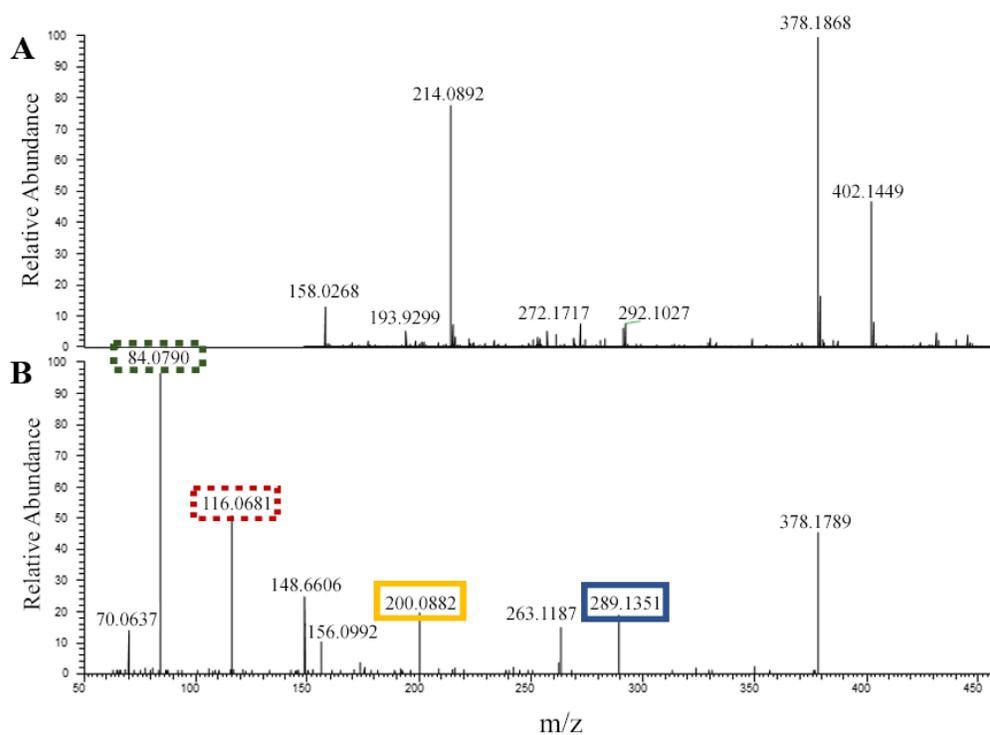
869   demonstrated.

870

871   **Figure 8. Neighbor-joining phylogenetic analysis of NIS synthetases**. A total of 24

872   experimentally validated and two proposed NIS-synthetases were aligned using MUSCLE

873   algorithm and the phylogenetic tree was constructed using SeaView. The code between

874   brackets corresponds with the NCBI accession number for each protein sequence. NIS-

875   synthetases are colored depending on their specificity of substrate and thus their group: A

876   (pink), A' (red), B (green), C (blue), C' (yellow). The enzymes presented in this study (*i.e.,*

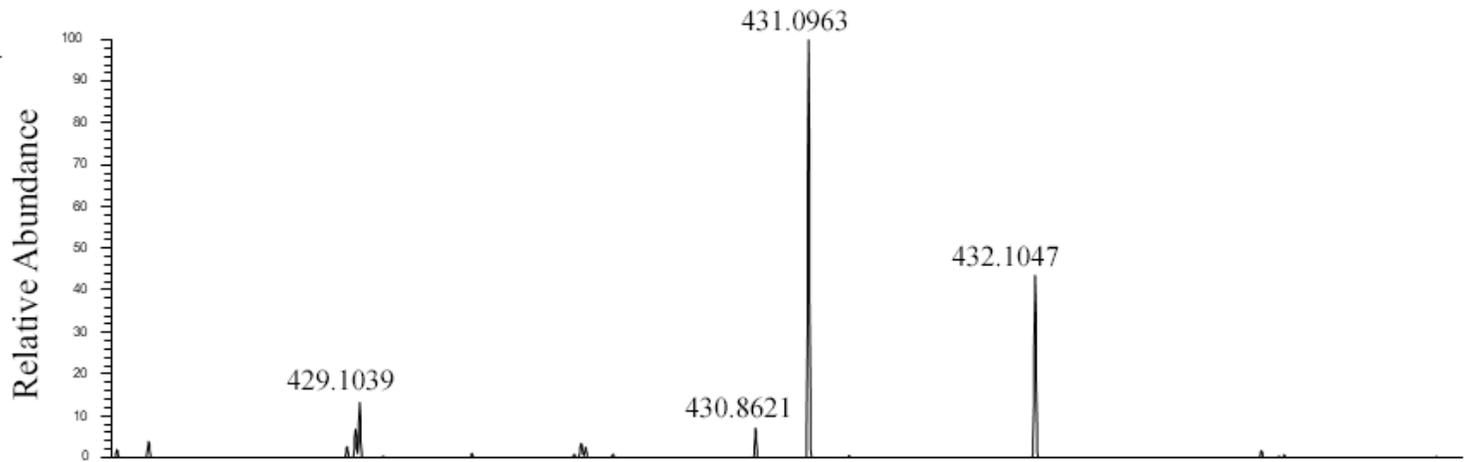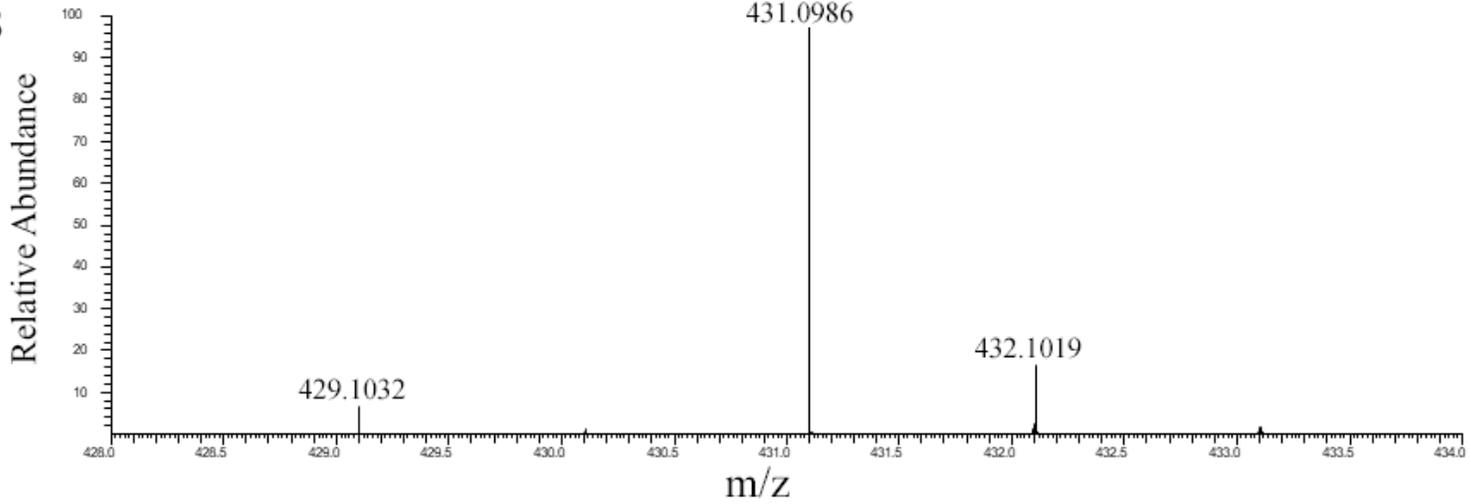877   RhiE and putative rhizobactin synthetases) are shown in black.

A WT growth

B *rhiE*::Gm growth

Iron concentration (mg/L) 0 0.5 1 5 10

A

Iron released into solution (mg/L)

- ■ + 200 mg Hematite (H)
- ▨ No mineral

a					

WT + H   WT   ΔrhiE + H   *rhiE*::Gm   Abiotic + H   Abiotic

B

A

Peak 1

B

Peak 2

Negative Control   *rhiE*::Gm   WT
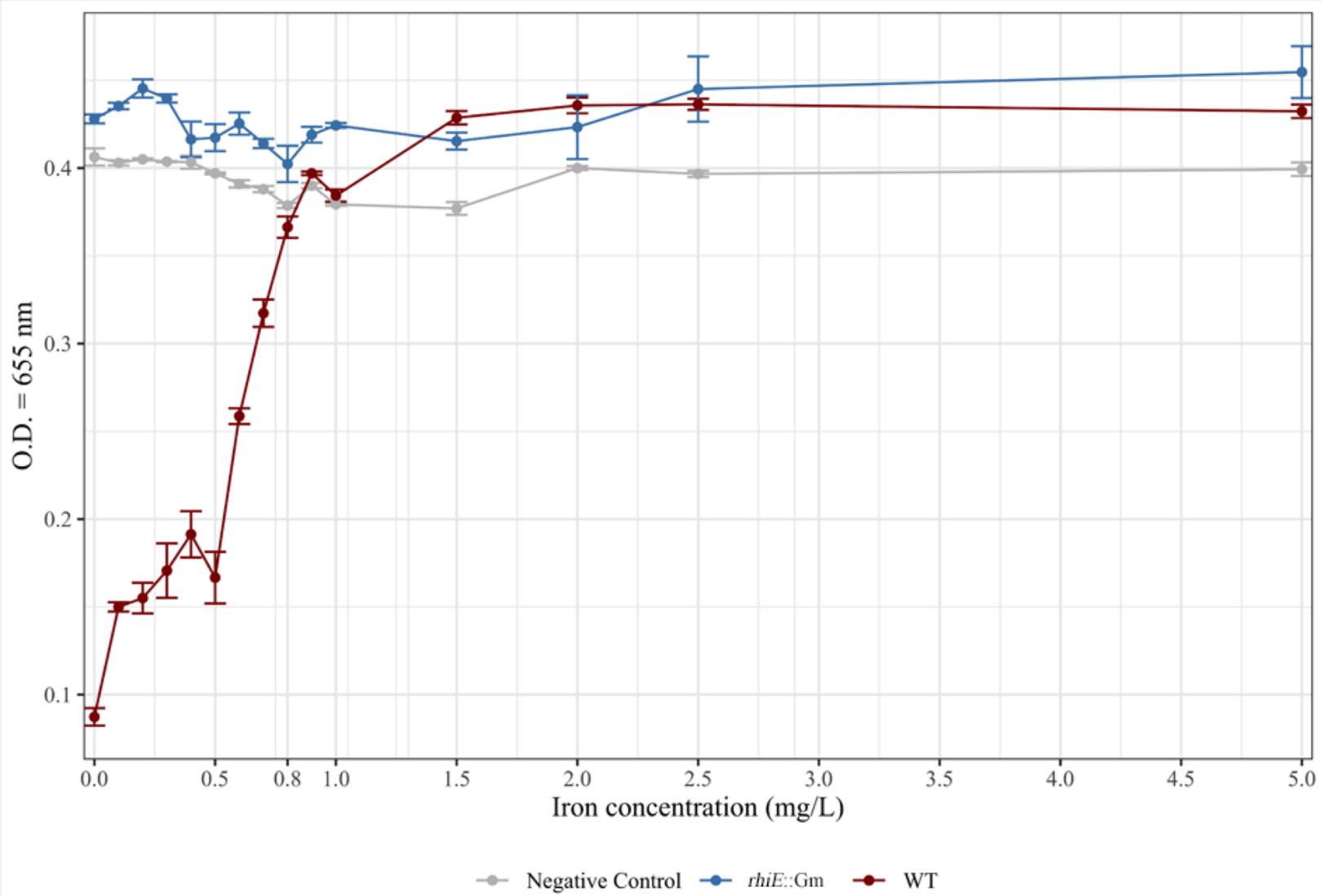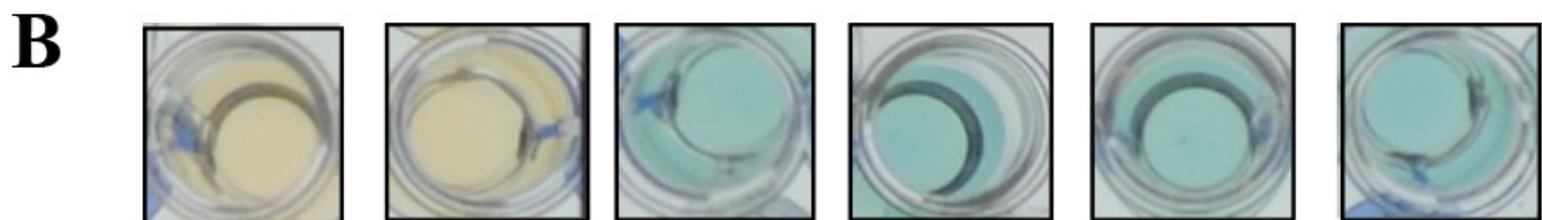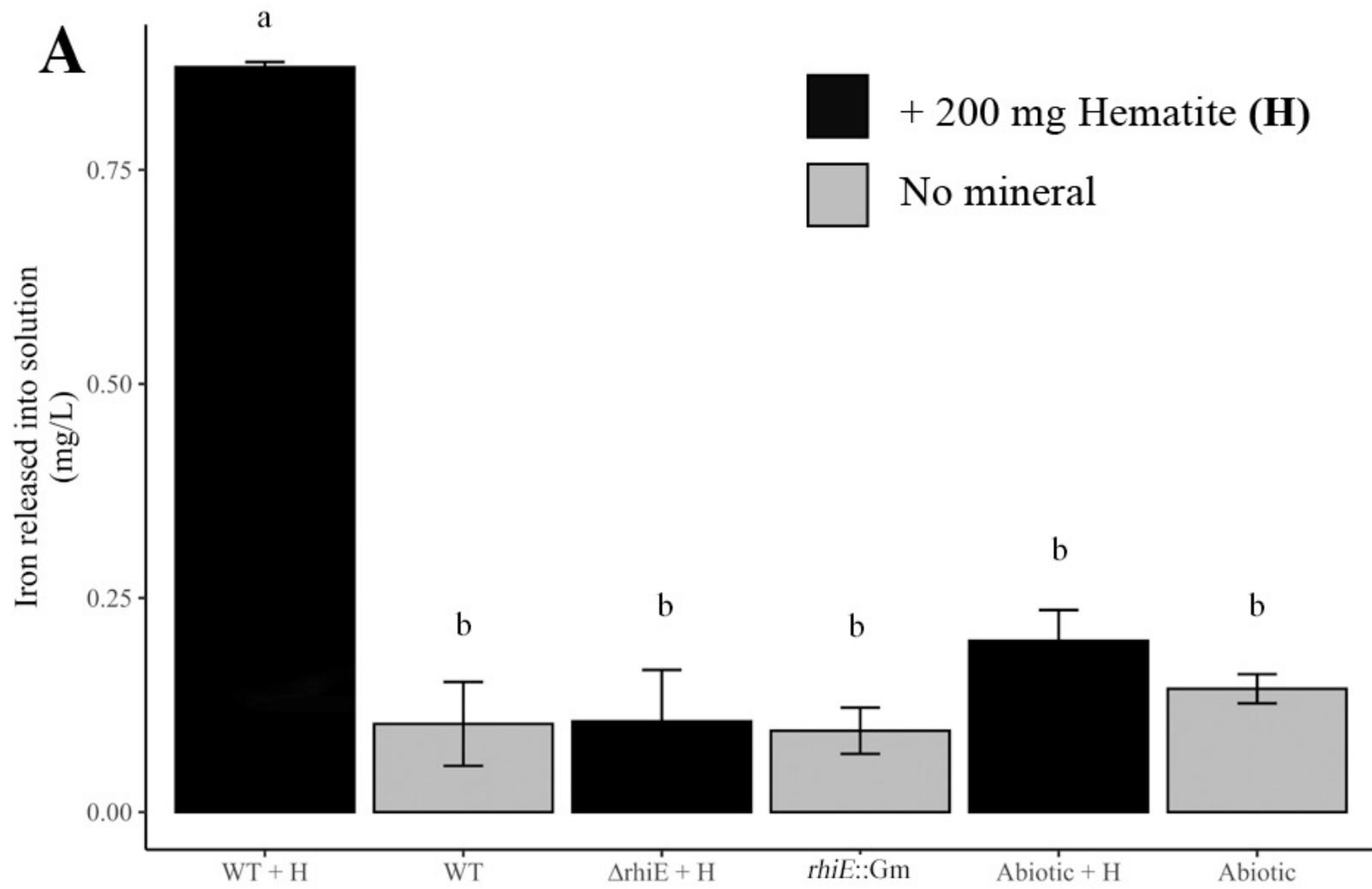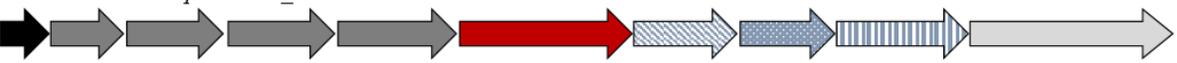
Caballeronia mineralivorans PML1 (12)

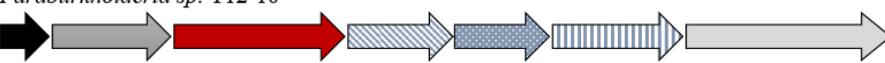*Paraburkholderia sp.* BL23I1N1

Paraburkholderia haematera

Paraburkholderia sp. NMBU_R16

Paraburkholderia sp. Ac-20340

Paraburkholderia sp. T12-10

Ensifer meliloti AK83

Pseudomonas sp. FEN

TonB-dependent siderophore receptor

Y4yA family PLP-dependent enzyme

Cysteine synthase family protein

NAD/NADP octopine/nopaline dehydrogenase family protein

iucA/iucC family siderophore biosynthesis protein

MFS transporter

ABC transporters

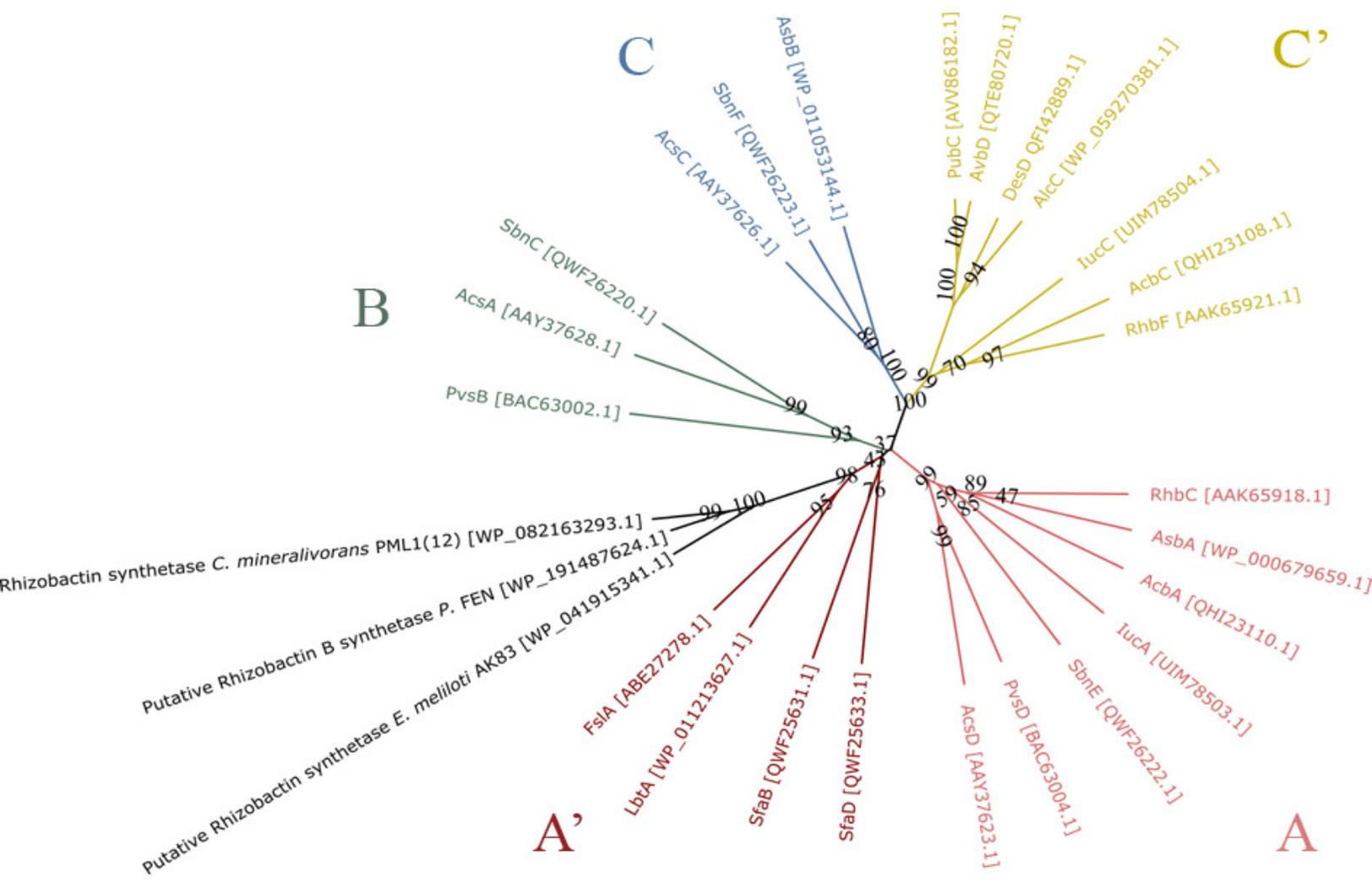Transcriptional regulator/GNAT family N-acetyltransferase

Ester-coA lyase

Table 1. **Description of the NRPS-independent gene region involved in siderophore production by *Caballeronia mineralivorans* strain PML1(12).** Each gene product of the cluster is presented by its NCBI accession number. The annotation is based on BLASTp homology. NIS synthetases showing the highest homology with RhiE of strain PML1(12) are shown.

Putative function	Accession number (NCBI)	Length	Gene	Annotation (based in BLASTp Homology)	Homology
Transport	KLU26370.1	745	*rhiA*	TonB-dependent siderophore receptor	88.19% *Paraburkholderia sp.* BL23IN1 (WP_120293907.1)
Synthesis	KLU26369.1	480	*rhiB*	Y4yA family PLP-dependent enzyme	80.62% *Paraburkholderia haematera* (CAE6738131.1)
Synthesis	KLU26368.1	346	*rhiC*	Cysteine synthase family protein	93.64% *Paraburkholderia sp.* BL23IN1 (WP_120293908.1)
Synthesis	KLU26367.1	388	*rhiD*	NAD/NADP octopine/nopaline dehydrogenase family protein	87.37% *Paraburkholderia haematera* (WP_236066808.1)
Synthesis	KLU26366.1	635	*rhiE*	*iucA/iucC* family siderophore biosynthesis protein	85.83% *Paraburkholderia sp.* BL23IN1 (WP_120293909.1)
Transport	KLU26365.1	421	*rhiF*	MFS transporter	85.34% *Paraburkholderia haematera* (WP_211611243.1) *Paraburkholderia sp.* BL23IN1 (WP_120293910.1)
Transport	KLU26364.1	398	*rhiG*	ABC transporter substrate-binding protein	88.69% *Paraburkholderia haematera* WP_211611244.1
Transport	KLU26363.1	353	*rhiH*	Iron ABC transporter permease	92.63% *Paraburkholderia sp.* BL23IN1 WP_120293912.1
Transport	KLU26362.1	265	*rhiI*	ABC transporter ATP-binding protein	92.83% *Paraburkholderia* sp. BL23IN1

					WP_120293913.1
Regulation	KLU26361.1	138	*rhiJ*	Transcriptional regulator/GNAT family N-acetyltransferase	87.71% *Caballeronia sordidicola* WP_031357714

Table 2. List of bacterial strains, constructions and primers used in this study.

Strains, plasmids, or primers	Characteristics	Reference
Strains		
Caballeronia mineralivorans		
Strain PML1(12)	Wild type strain	[18]
rhiE::Gm (PML1(12)(*rhiE*::Gm))	Wild type strain, with Gm^R cassette inserted in double crossing over	This study
Escherichia coli		
DH5α	*supE44*, Δ*lacU169*, (Φ*lacZ*ΔM15), *recA1, endA1, hsdR17, thi-1, gyrA96, relA1*	Lab collection
S17.1λpir	Tpr Sm^R *recA, thi, pro, hsdRM$^+$*, RP4::2-Tc::Mu::Km Tn7 λpir	Lab collection
Plasmids		
pUC1318	Amp^R, Gm^R	Lab collection
pGEM-T Easy	Amp^R	Kit Promega
pGEM-*rhiE*_SmaI	pGEM-T Easy carrying a *rhiE* gene	This study
pGEM-*rhiE*::Gm	pGEM-*rhiE*::Gm with insertion in *Sma*I of the Gm^R cassette	This study
pK19mob	Km^R	Lab collection
pK19mob-*rhiE*::Gm	pK19mob containing a *Eco*RI fragment obtained from pGEM-*rhiE*::Gm	This study
Primers (Tm = 54 °C)		
For_*rhiE*	5'- ATGAAGACCACTCCTTCGCTATT - 3'	This study
Rev_*rhiE*_*Sma*I	5'- GCACCGGTCCCGGGAGCCGCGGCAT - 3'	This study
For_*rhiE*_*Sma*I	5'- ATGCCGCGGCTCCCGGGACCGGTGC - 3'	This study
Rev_*rhiE*	5'- TCAACCCTCGTTGTGCGCCGCCAGC - 3'	This study

Gm^R, Km^R, Sm^R, and Amp^R, indicate gentamicin, kanamycin, spectinomycin and ampicillin resistance cassettes, respectively.